ORIGINAL ARTICLE

Formation of FeCrMoVC Layers on AA6061 by Laser Cladding Process: Microstructure and Wear Characteristics

N. Jeyaprakash[1,2] · Che-Hua Yang[1,2] · S. Sivasankaran[3]

Abstract Aluminium and its alloys (AA) are widely used in aerospace and automotive industries due to its superior properties such as stiffness to weight ratio and high strength. However, the less hardness and reduced wear resistance can limit their uses in several applications. In the present study, FeCrMoVC layers were formed on AA6061 material. Besides, the produced layers were investigated to reveal their new phase formation, hardness changes and microstructure. Sliding wear study was performed on both clad surface and base material. The wear mechanism and roughness average was evaluated and compared. The formed structure comprised of carbides and martensite with improved hardness. The wear resistance of the clad layer was improved 9 times better than base material. Abrasive, adhesive and delamination were the major wear mechanism on the base material while clad surface showed mild abrasive wear. The worn-out cladding surface showed three times lesser roughness while compared with base metal.

✉ N. Jeyaprakash
  prakash84gct@gmail.com; prakash@ntut.edu.tw

  Che-Hua Yang
  chyang@ntut.edu.tw

  S. Sivasankaran
  sivasankarangs1979@gmail.com; sivasankaran@qec.edu.sa

1 Centre of Mass Customization Additive Manufacture, National Taipei University of Technology, Taipei 10608, Taiwan ROC

2 Institute of Manufacturing Technology, National Taipei University of Technology, Taipei 10608, Taiwan ROC

3 Department of Mechanical Engineering, College of Engineering, Qassim University, Buraydah 51452, Saudi Arabia

1 Introduction

Aluminium and its alloys (AA) are widely used in automotive, aerospace and transportation industries due to its excellent properties such as high thermal conductivity, stiffness-to-weight ratio, high strength and good ductility [1]. However, the less hardness and reduced wear resistance can limit its uses especially for the situations where a hard surface is needed [2]. To enhance the surface-level properties, different surface alteration methods have been adopted and examined [3]. Thin reinforced layers can be formed through different surface alteration methods including plasma spraying [4], metal matrix composites [5], thermal spraying [6] and hard anodizing [7]. However, these deposition processes can be less considered due to their improper metallurgical bonding between base material and deposition [8].

Laser material processing is commonly used in most of the industries to enhance the surface-level properties of different metals such as copper [9], steel [10], magnesium [11] and titanium [12]. The produced laser beam reflects well directionality, high coherence and higher energy density [13]. Additional benefits of laser-based surface processing show the fact that the produced beam has a good spatial resolution which makes perfect coating on the surface. Laser-based surface modification includes laser surface alloying [14], laser surface melting [15] and laser surface cladding [16]. The produced high-power laser source can melt both alloy powders and base material to form good metallurgical bonding [17]. Furthermore, laser surface processing comprises of rapid heating/cooling and

higher gradients which can form the metastable phases with different microstructures that cannot be formed through any other conventional surfacing methods [18]. This reformed microstructure can enhance the mechanical and tribological properties without damaging the base material.

Bhujanga et al. [19] studied the wear behaviour of B_4C reinforced on AA6061 through metallurgical route and concluded that adding B_4C into AA6061 surface increased the hardness, wear resistance and tensile strength. Mir Irfan Ul Haq and his co-worker [20] has reviewed the reinforcement of titanium diboride on aluminium alloys such as AA 2014, AA 2219, AA 6061, AA 7075, and AA 6063 surface and concluded that mechanical and tribological properties were improved to 60%. Shiqiang Qian et al. [21] examined the nano-composite coating on aluminium alloy using plasma transferred arc (PTA) method and concluded that surface-modified aluminium alloy improved the hardness and corrosion resistance. Based on the literature, there are many deposition methods such as PTA, metallurgical route and laser alloying were used to improve the surface properties. Besides, limited studies were focussed on laser cladding process. However, no literature can be found on the laser cladding of AA6061 with H13 steel powder which has focused on phase analysis, microstructural, hardness, wear properties and their detailed relationships. In the present study, the microstructural formation of laser cladding surface, phase analysis, hardness, wear properties and roughness averages were studied.

2 Experimental Procedure

An AA6061 circular rod with the dimensions of 2.5 cm diameter X 3 cm length was used as base material. The surface of base material was sand blasted to obtain a higher bond strength between base metal and coating material. The used premixed alloy powders were FeCrMoVC (H13 steel) with the particle size of 30–140 microns. The chemical composition of base material and selected powders are given in Table 1.

A 4 kW Yb: YAG disc laser was used to deposit the alloy powders on the base material. The cladding

Table 2 Laser cladding parameters

Power	1300 (watts)
Scanning speed	400 /min
Feed rate	4 g/min
Spot size	3.2 mm
Stand-off	15 mm
Preheating	150 °C
Overlapping	50%
Powder carrier gas (argon)	6 SD@1 bar
Shielding gas (argon)	25 lpm

parameters such as scanning power (w), powder flow rate (g/min) and travel speed (mm/min) were varied and suitable parameters were identified based on the defect-free surface (Table 2). The laser-cladded samples were cross-sectioned to study their structure and hardness. The coating thickness (600 microns) was measured with optical microscopy (OM) (Olympus) and FE-SEM (JEOL-JSM-7610F) with EDS was used to analyse their microstructure. Figure 1a–c shows the SEM image of alloy powder, schematic of laser cladding process and macro picture of specimen after cladding. X-ray analysis was performed on the cladded surface and powders to expose their new phase formation. Further, hardness test was performed on the cladded region and base material to identify the changes using Vickers hardness tester. Dry sliding pin-on-plate wear experiment was performed to analyse the wear properties on both base metal and cladded surface as per ASTM G99-05 standard [22]. Hardened steel disc was used as counterpart with the dimensions of 100 mm diameter and 6 mm thickness. The selected tribological parameters were load (20 N), total sliding distance (1500 m) and velocity (1 m/s). The mass loss of base material and cladded specimen was measured before and after the wear study. Besides, material removal mechanism and worn-out surface roughness average were examined using FE-SEM and white light interferometer, respectively.

Table 1 Chemical composition of substrate and powder

Materials	Elements composition (wt %)											
	Ni	Co	Cr	Fe	Al	C	Si	Mo	Ti	Mn	Mg	V
Substrate (AA6061)	–	0.35	0.31	0.75	REM	–	0.50	–	0.12	1.1	0.95	–
FeCrMoVC	0.35	–	5.1	REM	–	0.36	1.2	1.53	–	0.52	–	1.4
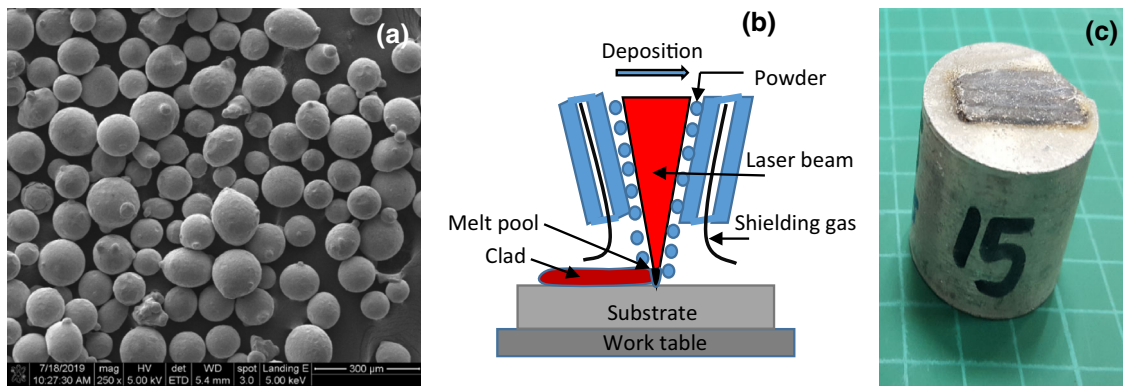
Fig. 1 SEM picture of used alloy powders (**a**), schematic of laser cladding process (**b**), and macropicture of specimen after cladding (**c**)

3 Results and Discussion

3.1 Microstructure and Hardness Analysis

OM and SEM picture (Fig. 2) of the samples show that FeCrMoVC powders are successfully coated on AA6061 surface. The cross-sectioned surface shows three different regions likely cladded, interface and substrate as shown in Fig. 2a. The deposition shows that there are no defects such as cracks and pores. The interface regions show sharp transition between base material and cladding. The produced heat source penetrates into substrate material and simultaneously the rate of cooling is minimized and forms the heat-affected region between substrate and clad. When heat source travels into substrate, the coated area solidifies quickly with iron contents. The amorphous structure is formed due to proper adjustment of heat source and solidification rate. After laser deposition, martensite structure is created due to rapid cooling of coating [23]. As indicated in Fig. 2b, the laser-cladded H13 structure includes large sized carbides, martensite and fine-grained pearlite [24]. The laser cladded region indicates eutectic carbides. The vanadium carbides (VC) are uniformly distributed on coating region and this can improve the wear properties of the cladded layer. The distributed carbide element minimizes the variations in the microhardness and reduces the carbide pull out. In HAZ, the observed images indicating needle-like lengthy grains are observed (Fig. 2c). The EDS analysis indicated the presence of various elements such as Mo, Cr, VC, and Fe. Figure 2c, d shows the SEM picture of magnified HAZ, and elemental analysis of cladding region, respectively.

Figure 3a shows the microhardness profile of laser cladding with indentation picture. There are three various regions, namely cladded area, heat-affected zone (HAZ) and substrate. It can be observed that the laser-cladded area shows higher hardness values than substrate. The presence of elements such as vanadium and molybdenum are the major reason for the improved hardness due to the formation of strong carbides on the cladded region [25]. Further, the formation of martensite, less carbides of alloying contents such as chromium, molybdenum also supports to improve the strength and hardness of laser-cladded region [26]. Carbides and martensites are expected to form during the laser cladding with steel powders. The formed carbides and martensites during laser cladding process are significantly finer due to rapid cooling and solidification. This has been verified practically that while depositing hard elements on the softer region, the strength and hardness of the deposited layer get improved [3]. Besides, the inset picture represents the indentation size captured during hardness analysis. In cladded surface, the observed indentation size is small as compared to heat-affected zone indentation. The noticed small sized indentation reveals that it is capable of bearing higher external loads while compared with greater sized indentation with the same input parameters of 300 g load and 15 s dwell time [27].

3.2 Phase Analysis

Figure 3b shows the phase diagram of powder and cladding surface. It can be noticed that the laser cladding surface shows higher α-ferrite peaks (ICDD:00-006-0696) than as received powder (ferrite phase, ICDD: 00-033-0397). The formed ferrite phase may also include martensite phase ($C_{0.14}Fe_{1.86}$, ICDD:00-044-1289) along with finer structure which is produced through laser cladding that could be the reason for the improved microhardness [28]. Further, the peaks related to substrate (α-Al, ICDD: 00-001-1176) are also observed. During number of passes, the temperature influences the peak intensity and decreases with the increase in the carbides. However, during laser cladding with high temperature, the coating surface is completely altered and various structures are created which is recognized through X-ray analysis [29].
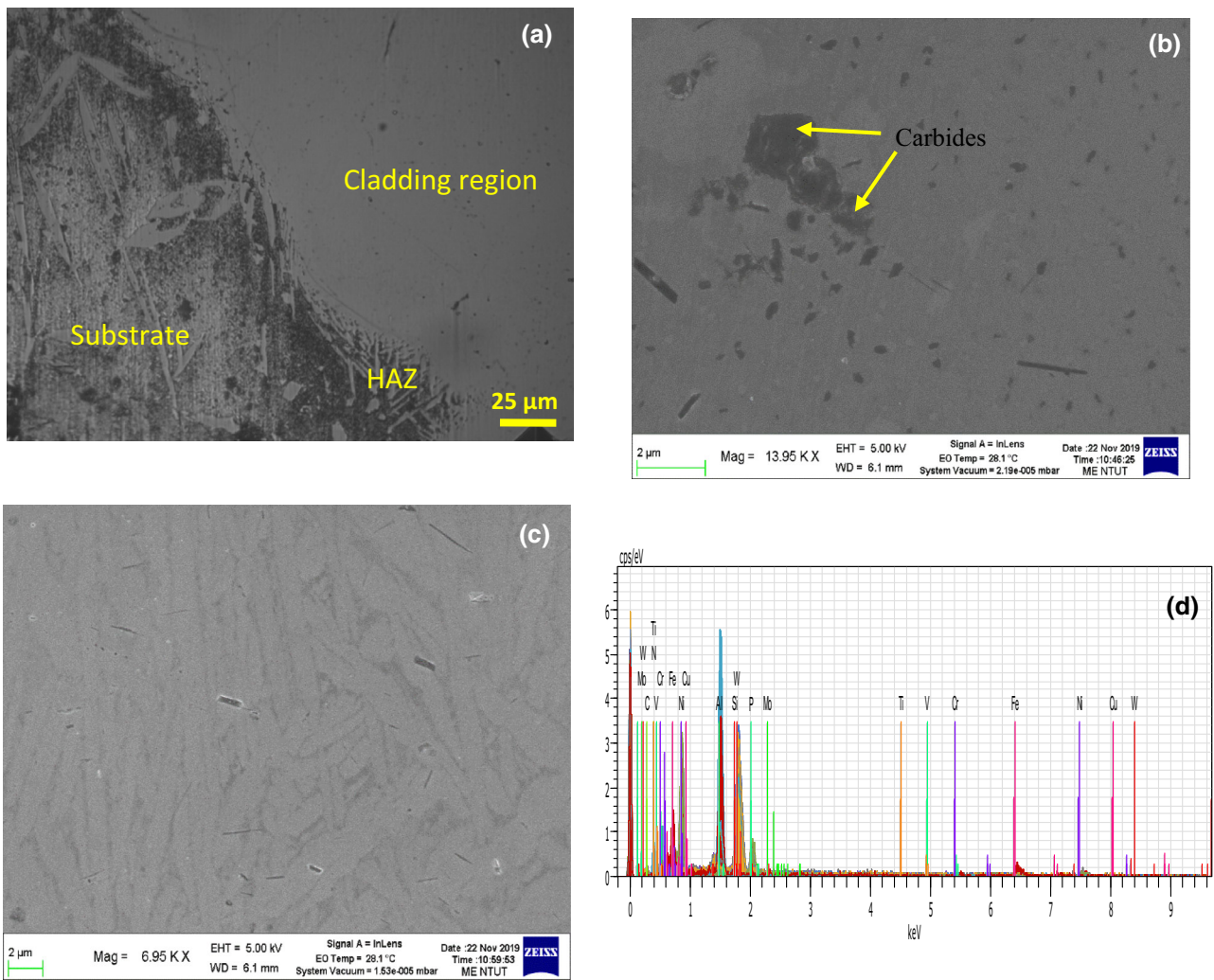
Fig. 2 OM picture of various regions namely cladding, HAZ and substrate (**a**), SEM picture of cladding centre region (**b**), SEM picture of magnified HAZ (**c**), and elemental analysis of cladding region (**d**)
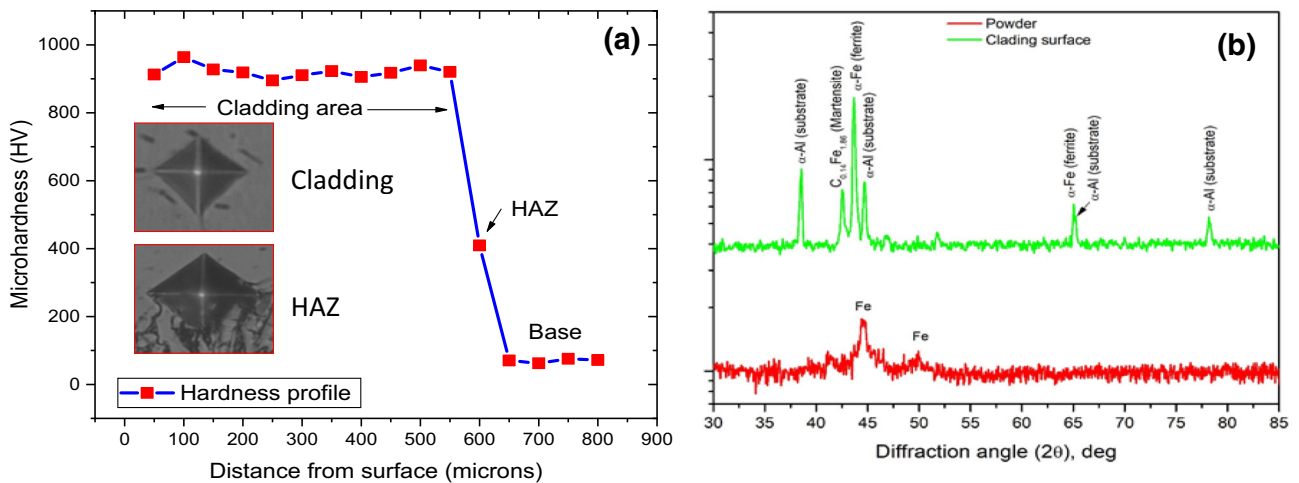
Fig. 3 Microhardness profile with indentation (**a**), phase analysis of substrate and cladding surface (**b**)

3.3 Tribological Study

Figure 4a represents the material loss against total sliding distance of the base material and clad specimen. It can be observed that the substrate shows severe wear with abrasive particle. There are larger debris present on the substrate surface, and the material is removed layer by layer. The material loss for substrate specimen is higher than cladded specimen. The formed carbides improve the wear resistance of the clad surface while sliding on the steel counterpart. The wear behaviour of substrate and clad samples show similar trend; while increasing the sliding distance, the mass loss also get increased. The improved wear resistance is noticed on the clad specimen due to evenly distributed hard carbides on the clad layer. In fact, the tough carbides delay the transition load in such a way that the material loss of the deposited specimen is significantly minimized [30]. The used machine is pin-on-disc abrasive wear tester, and the load carrying capacity of formed hard structure is a major factor in the wear resistance improvement. In this study, 500 g load has been applied and investigated. Normally in aluminium alloy, the load is applied at the beginning and then applied regularly onto the harder steel disc due to soft surface deformation. The steel counterpart is able to plough the material from the softer surface and cause microlevel cutting. In another side, the hard microns deposited on the load-bearing system can greatly reduce the microcutting and material loss [31]. In most of the cases, the hardness of the material directly affects the wear resistance of the material. It specifies the greater microhardness, the increased wear resistance and minimized total mass loss. The reduced wear rate of the deposited layer is combined with the effects of hard particles and softer matrix of aluminium.

Additionally, the good bond strength of coating and substrate causes lesser material loss [32].

Coefficient of friction (CoF) is the efficient way to examine the wear resistance of the material. Generally, the minimized CoF greatly improves the wear resistance of the material. The observed CoF of base material and clad with FeCrMoVC particle is given in Fig. 4b. It can be observed from the CoF plot that the base material starts from 0.61 and reaches maximum to 0.72. However, the clad surface friction starts from 0.31 and reaches maximum to 0.53. The hard carbides of the coating reduces the CoF significantly. This kind of strong carbides protect the specimen surface from the sudden or unpredicted damages. Thus, the material loss and frictional force is greatly reduced for the clad surface than substrate.

3.4 Wear Mechanism and Roughness Average

In order to study the wear mechanisms of the worn-out samples, SEM investigation is performed on worn surfaces. It can be noticed that the worn surfaces of substrate show deep and lengthy grooves, where the material is detached from the unclad softer surface during sliding wear test. Figure 5a shows the worn-out surface of the substrate material. The observed major wear mechanism is abrasive, adhesive and delamination. The material removed from the laser-modified surface by pressing the harder counterpart with an applied load causes abrasive wear. The bonding between laser modified and counterpart surface causes the metal transfer from the weaker surface to stronger surface (adhesive) and continuous to delaminate. At the initial stage, the removed material is less and indicates abrasive wear with small debris. While increasing the sliding distance, the material removal rate is increased by pulling the
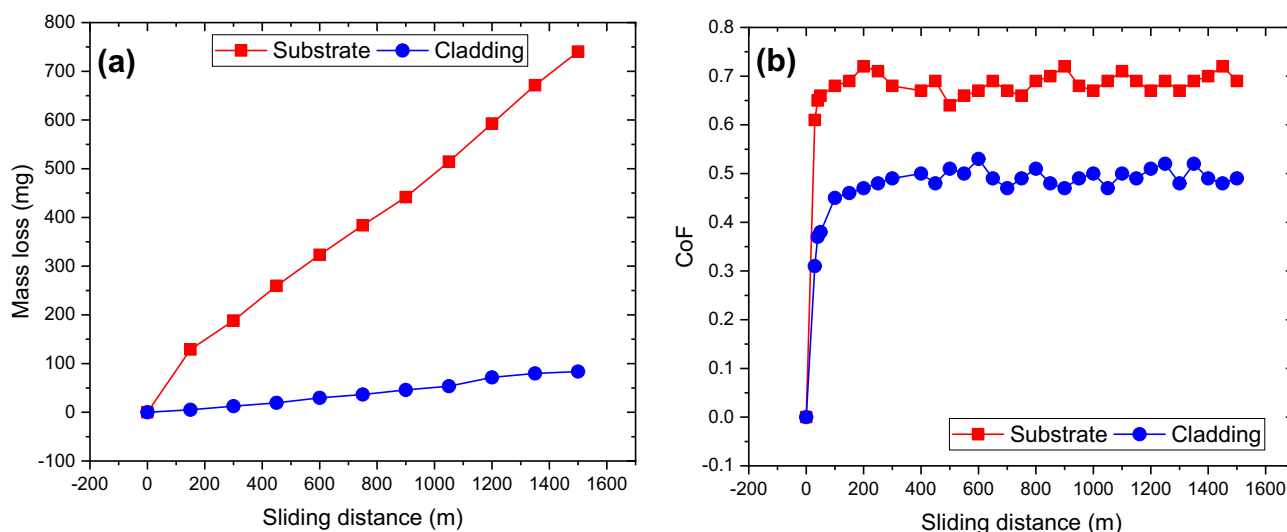

Fig. 4 Mass loss (a), Coefficient of friction (b) for both substrate and cladding specimen

material from the softer surface. The harder disc is pressed on the softer surface thus pulling out materials which indicates the adhesive wear and some particles are delaminated. Severe wear is noticed on the substrate material showing the total mass loss of 740 mg. The corresponding roughness average (Ra) is measured on the worn-out surface of the substrate and it shows 6.5 μm. Figure 5b shows the 3D profile and its corresponding roughness graph of worn-out base metal surface. The worn surface of laser clad sample shows less cutting grooves while compared to substrate surface. So, the material loss reduces on the clad surface due to existence of hard carbides and improve the wear resistance significantly. Figure 5c shows the worn-out surface of clad specimen. The hard carbides have higher resistance against microlevel cutting process and reduces the mass loss of the specimen [30]. However, the mild abrasive wear can be noticed on the clad surface while pressing the hard disc on the surface. The developed clad layers included with VC particles provide greater wear resistance. Besides, the refined
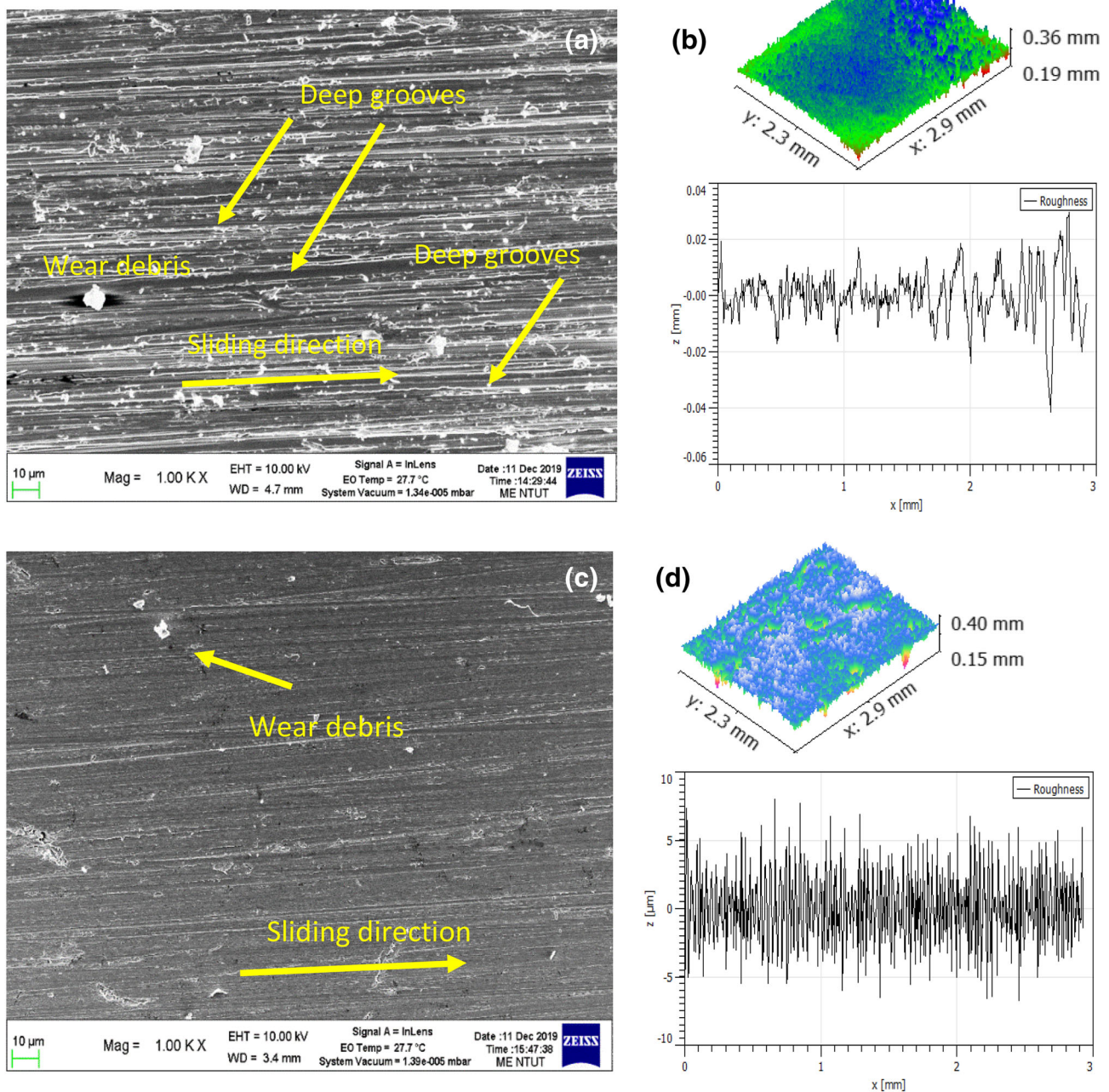
Fig. 5 Worn-out surface of (a) substrate, (c) cladding and their corresponding roughness average (b, d)

structure enhances the hardness of clad layer, and keeps the finer carbides while increasing the sliding distance. The improved hardness and reduced material loss results in lesser roughness average (Ra) of 2.1 μm. The clad worn-out surface shows three times lesser roughness when compared to substrate worn-out surface. Figure 5d shows the 3D profile and its corresponding roughness graph of worn-out clad surface.

4 Conclusion

In this study, laser cladding was performed on AA6061 surface to expose their microstructure, phase formation and wear resistance. The following conclusions could be drawn from the obtained results.

- The structure of laser-cladded surface included large size carbides and martensites. The vanadium carbides were uniformly distributed on the coating region and improved the wear resistance.
- The presence of vanadium and molybdenum was a major reason for the improved hardness due to formation of strong carbides on the cladded region. The laser cladding temperature influenced the peak intensity and decreased with the increase in the carbide contents.
- The material loss for substrate specimen was higher than cladded specimen. The formed carbides improve the wear resistance of the clad surface while sliding on the steel counterpart. The frictional force was greatly reduced for the clad surface than substrate.
- Severe wear was noticed on the substrate material which indicated abrasive, adhesive and delamination, while clad surface showed mild abrasive wear. The clad worn-out surface showed three times lesser roughness average when compared with base metal.

References

1. Shanmugasundaram A, Sanjivi A, and Sellamuthu R, *Trans Indian Inst Met* **71** (2018) 117.
2. Huang KJ, Lin X, Xie CS, and Yue TM. *J Wuhan Univ Technol Mater* **23** (2008) 89.
3. Jeyaprakash N, Muthukannan D, and Aditya SV, *Surf Rev Lett* **25** (2018) 1950009.
4. Peihu G, Jianping L, Zhong Y, Yongchun G, and Yanrong W, *Rare Metal Mat Eng* **44** (2015) 2396.
5. Bansala P, and Upadhyay L, *Procedia Eng* **51** (2013) 818.
6. Picas JA, Forn A, Rilla R and Martín E, *Surf Coat Technol* **200** (2005)1178.
7. Choudhary RK, Mishra P, Kain V, Singh K, Kumar S, and Chakravartty JK, *Surf Coat Technol* **283** (2015) 135.
8. Zhang QY, Li XQ, Wang DY, Tian YS, and Aleem BJA, *Mater Heat Treatment* **39** (2010) 120.
9. Yan H, Zhang PL, Yu ZS, Lu QH, Yang SL, and Li CG, *Surf Coat Technol* **206** (2012) 4046.
10. Jeyaprakash N, Yang CH, and Tseng SP, *Met Mater Int* (2019) https://doi.org/10.1007/s12540-019-00526-6.
11. Yue TM, Xie H, Lin X, Yang HO, and Meng GH, *J Alloy Compd* **587** (2014) 588.
12. Jeyaprakash N, Yang CH, and Tseng SP, *Int J Adv Manuf Technol* **106** (2019) 2347.
13. Xiao RS, and Zhang XY, *J Manuf Process* **16** (2014)166.
14. Jeyaprakash N, Yang CH, Muthukannan D and Prabu G, *Results Phys* **12** (2019) 1610.
15. Pagano N, Angelini V, Ceschini L, and Campana G, *Procedia CIRP* **41** (2016) 987.
16. Jeyaprakash N, Yang CH, and Sivasankaran S, *Mater Manuf Process* 35 (2020) 142.
17. Liu Z, Chong PH, Skeldon P, Hilton PA, Spencer JT, and Quayle B, *Surf Coat Technol* **200** (2006) 5514.
18. Petrović S, Radak B, Peruško D, Pelicon P, Kovač J, Mitrić M, Gaković B and Trtica M, *Appl Surf Sci* **264** (2013) 273.
19. Bhujanga DP, and Manohara HR, *Mater Today Proc* **5** (2018) 19773.
20. Singh H, Raina A, and Haq MIU, *Mater Today Proc* **5** (2018) 17982.
21. Wang W, Qian S, and Zhou X, *Trans Non-ferrous Met Soc China* **19** (2009) 1180.
22. Standard test method for wear testing with a pin-on-disk apparatus, ASTM Standard (2010) G: 99-05.
23. Van Bohemen, SMC, and Sietsma J, *Metall Mater Trans A* **40A** (2009) 1059.
24. Ning A, Mao W, Chen X, Guo H and Guo J, *Metals* **7** (2017) 70.
25. Li S, Wu X, Chen S, and Li J, *J Mater Eng Perform* **25** (2016) 2993.
26. Verhoeven JD, *Steel Metallurgy for the Non-metallurgist*, ASM International, Cleveland 2007.
27. Liu R, Yao J, Zhang Q, Yao MX, and Collier R, *J Eng Mater Technol* **138** (2016) 041001.
28. Telasang G, Majumdar JD, Padmanabham G, and Manna I, *Mater Sci Eng A* **599** (2014) 255.
29. Karmakar DP, Muvvala G, and Nath AK, *Surf Coat Technol* **361** (2019) 136.
30. Chong PH, Man HC, and Yue TM, *Surf Coat Technol* **145** (2001) 51.
31. Wang AG, and Hutchings IM, *Mater Sci Technol* **5** (1989) 71-76.
32. Chong PH, Man HC, and Yue TM, *Surf Coat Technol* **154** (2002) 268.